HHS Public Access

Author manuscript

Mol Pharm. Author manuscript; available in PMC 2021 March 15.

Published in final edited form as:

Mol Pharm. 2020 September 08; 17(9): 3392–3402. doi:10.1021/acs.molpharmaceut.0c00457.

Development of 5D3-DM1: A Novel Anti-Prostate-Specific Membrane Antigen Antibody-Drug Conjugate for PSMA-Positive Prostate Cancer Therapy

Colin T. Huang,
The Russell H. Morgan Department of Radiology and Radiological Science, The Johns Hopkins University School of Medicine, Baltimore, Maryland 21205, United States

Xin Guo,
Department of Molecular and Comparative Pathobiology, The Johns Hopkins University School of Medicine, Baltimore, Maryland 21205, United States

Cyril Bařinka,
Laboratory of Structural Biology, Institute of Biotechnology of the Czech Academy of Sciences, BIOCEV, 252 50 Vestec, Czech Republic

Shawn E. Lupold,
The James Buchanan Brady Urologic Institute and Department of Urology, Johns Hopkins School of Medicine, Baltimore, Maryland 21287, United States

Martin G. Pomper,
The Russell H. Morgan Department of Radiology and Radiological Science and Department of Oncology, the Sidney Kimmel Comprehensive Cancer Center, The Johns Hopkins University School of Medicine, Baltimore, Maryland 21205, United States; The James Buchanan Brady Urologic Institute and Department of Urology, Johns Hopkins School of Medicine, Baltimore, Maryland 21287, United States

Kathleen Gabrielson,
Department of Molecular and Comparative Pathobiology, The Johns Hopkins University School of Medicine, Baltimore, Maryland 21205, United States

Venu Raman,
The Russell H. Morgan Department of Radiology and Radiological Science and Department of Oncology, the Sidney Kimmel Comprehensive Cancer Center, The Johns Hopkins University School of Medicine, Baltimore, Maryland 21205, United States

Dmitri Artemov,

Corresponding Author: Phone: +1(443) 287-4426; shapuar1@jh.edu; Fax: +1(410) 614-1948.

The authors declare no competing financial interest.

ASSOCIATED CONTENT

Supporting Information

The Supporting Information is available free of charge at https://pubs.acs.org/doi/10.1021/acs.molpharmaceut.0c00457.
Fluorescence images of 5D3, anti-AXL, and trastuzumab mAbs in PC3-PIP, MDA-MB-231, and BT-474 cancer cells; PC3-Flu cells treated with 5D3-DM1; MALDI-TOF spectra showing the stability of 5D3-DM1; graphs of PLT and WBC levels in treated and untreated mice; and an image of metastatic tumors found on the kidneys of an untreated mouse (PDF)
Complete contact information is available at: https://pubs.acs.org/10.1021/acs.molpharmaceut.0c00457

The Russell H. Morgan Department of Radiology and Radiological Science and Department of Oncology, the Sidney Kimmel Comprehensive Cancer Center, The Johns Hopkins University School of Medicine, Baltimore, Maryland 21205, United States

Sudath Hapuarachchige
The Russell H. Morgan Department of Radiology and Radiological Science, The Johns Hopkins University School of Medicine, Baltimore, Maryland 21205, United States

Abstract

Prostate cancer (PC) is a potentially high-risk disease and the most common cancer in American men. It is a leading cause of cancer-related deaths in men in the US, second only to lung and bronchus cancer. Advanced and metastatic PC is initially treated with androgen deprivation therapy (ADT), but nearly all cases eventually progress to castrate-resistant prostate cancer (CRPC). CRPC is incurable in the metastatic stage but can be slowed by some conventional chemotherapeutics and second-generation ADT, such as enzalutamide and abiraterone. Therefore, novel therapeutic strategies are urgently needed. Prostate-specific membrane antigen (PSMA) is overexpressed in almost all aggressive PCs. PSMA is widely used as a target for PC imaging and drug delivery. Anti-PSMA monoclonal antibodies (mAbs) have been developed as bioligands for diagnostic imaging and targeted PC therapy. However, these mAbs are successfully used in PC imaging and only a few have gone beyond phase-I for targeted therapy. The 5D3 mAb is a novel, high-affinity, and fast-internalizing anti-PSMA antibody. Importantly, 5D3 mAb demonstrates a unique pattern of cellular localization to the centrosome after internalization in PSMA(+) PC3-PIP cells. These characteristics make 5D3 mAb an ideal bioligand to deliver tubulin inhibitors, such as mertansine, to the cell centrosome, leading to mitotic arrest and elimination of dividing PC cells. We have successfully developed a 5D3 mAb- and mertansine (DM1)-based antibody-drug conjugate (ADC) and evaluated it *in vitro* for binding affinity, internalization, and cytotoxicity. The *in vivo* therapeutic efficacy of 5D3-DM1 ADC was evaluated in PSMA(+) PC3-PIP and PSMA(–) PC3-Flu mouse models of human PC. This therapeutic study has revealed that this new anti-PSMA ADC can successfully control the growth of PSMA(+) tumors without inducing systemic toxicity.

Graphical Abstract

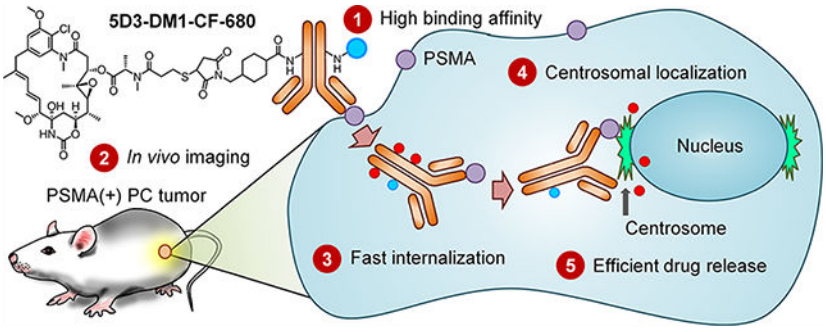

Keywords

prostate cancer; prostate-specific membrane antigen (PSMA); drug delivery; targeted therapy; antibody-drug conjugates (ADC); MCC linker; anti-PSMA antibody; 5D3 antibody; mertansine (DM1)

1. INTRODUCTION

In the USA, prostate cancer (PC) is the most common cancer in men and the second leading cause of cancer-related death after lung and bronchus cancer. Over 174,000 American men were diagnosed with PC last year, and 18% of PC patients die yearly from this devastating decease.[1,2] Androgen deprivation therapy is initially effective in most metastatic PCs, but PCs eventually become resistant to hormone-based therapeutics and progress into castrate-resistant prostate cancer (CRPC).[3,4] At this stage, CRPC has typically metastasized to the bone and eventually to other vital organs of the body.[5] Second-line chemotherapeutics and hormone ablation therapies, such as docetaxel and enzalutamide and abiraterone, can extend survival; however, approximately 15–25% of patients will not respond to second-line therapy.[6,7] Novel targeted therapeutics are urgently needed to improve metastatic CRPC treatment by enhancing therapeutic efficacy and minimizing systemic toxicity.

Prostate-specific membrane antigen (PSMA) is an integral membrane protein with a molecular weight of 110 kDa and consisting of 750 amino acids.[8] PSMA is overexpressed in practically all malignant PC tumors compared to non-prostatic tissues.[9,10] It is also known that cancer aggressiveness, androgen blockage, and deprivation enhance PSMA expression levels.[11,12] Following binding by bioligands, such as anti-PSMA monoclonal antibodies (mAbs), low-molecular weight compounds, and peptides, PSMA is readily internalized.[13,14] These characteristics make PSMA a perfect target for the development of diagnostic imaging probes and targeted therapeutics for PC.[15–18]

7E11 was the first anti-PSMA antibody originally developed using LNCaP PC cells as an antigen. The 7E11 mAb binds to the intracellular epitope of PSMA that is only exposed in apoptotic or necrotic PC cells.[19–21] Therefore, 7E11 mAb can be used as a bioligand for imaging PC but not for targeted therapy. Following the development of 7E11, a series of anti-PSMA mAbs were developed that targeted the extracellular moiety of PSMA. Some of anti-PSMA mAbs have been humanized, making them feasible for diagnosis or therapy without inducing the anti-mouse immune response. Among them, the humanized J591 mAb (HuJ591) was the most successful mAb, to date, with high binding affinity to the extracellular moiety of PSMA, and is widely used for PC imaging and radiotherapy. Following PSMA binding, the J591-PSMA complex internalizes quickly and localizes to endosomes in the cells, which enables efficient delivery of chemotherapeutics to the target cell. MLN2704 is an antibody-drug conjugate (ADC) that utilizes the anti-PSMA characteristics of HuJ591 for the targeted drug delivery of the anti-tubulin agent, mertansine (DM1), in PC therapy. However, MLN2704 has a narrow therapeutic window in metastatic CRPC therapy because of the poor stability of the disulfide linker.[22]

5D3 is a mAb that specifically binds to the extracellular domain of PSMA with sub-nanomolar affinity. This mAb has been previously used for targeted-imaging of PSMA(+) PCs.[23] By comparison, the binding affinities of 5D3 and J591 mAbs to PSMA are 0.14 and 1.2 nM, respectively, as determined by enzyme-linked immunosorbent assay. 5D3 mAb exhibits improved characteristics as a bioligand for targeting PC because of a nearly 10-fold higher binding affinity compared to J591.[24]

We have recently used 5D3 mAb for pretargeting therapy in PSMA(+) PC cells by the sequential treatment of 5D3-based pretargeting components, followed by a drug delivery component, which recognizes two components on the targeted cell surface by *trans*-cyclooctene-tetrazine bioorthogonal click chemistry.[25] Our proof-of-concept study revealed interesting results *in vitro*, showing a significant reduction of cell viability in PSMA(+) PC3-PIP PC cells compared to PSMA(–) PC3-Flu cells.[25] However, in animal models, an 8–24 h period is required to clear the unbound mAb from circulation before the second drug delivery component can be administered. Our *in vitro* studies revealed that 75% of surface-bound 5D3 mAbs are internalized within the first 2 h and remained inside cells for more than 24 h.[25] Within this time-frame, surface-bound 5D3 mAbs are internalized and not available on the cell surface. High binding affinity, fast internalization, and prolonged persistence of 5D3 in the cytoplasm are ideal factors for the development 5D3-based anti-PSMA ADCs for the therapy of PSMA(+) PC.

Our studies have also revealed that 5D3 mAb has a unique pattern of internalization in the target PC cells and it localizes to the centrosomal compartment in the vicinity of the nucleus. The centrosome is a cytoplasmic organelle, which serves as an organizing center for microtubule growth during the interphase of mitosis. Therefore, the 5D3 mAb can be conjugated with anti-tubulin drugs, such as mertansine (DM1) and paclitaxel, to directly deliver these agents to the centrosome and induce mitotic arrest and killing of cancer cells. Hence, our target-specificity is not limited to targeting PSMA(+) receptors on PC cells but also applies to specific delivery of drugs to the centrosome that is vital for cell division.

DM1 is used as a chemotherapeutic for ADC development and was discovered in the *Maytenus ovatus* shrub.[26–28] It is an anti-tubulin agent that inhibits the assembly of microtubules leading to the induction of mitotic arrest and the killing of cells at sub-nanomolar concentrations.[29] The antimitotic effects of maytansine derivatives are linked to their ability to bind to tubulin, inhibiting microtubule assembly.[30] DM1 is not target-specific and can attack healthy tissues as well, resulting in severe side effects and systemic toxicity.[31] To circumvent the lack of specificity, DM1 is typically conjugated to a target-specific antibody to be used as an ADC. The drug thiol functional group can be used for standard conjugation with antibodies without a reduction in toxicity. The unique characteristics of anti-PSMA 5D3 mAb: high target-specificity, enhanced binding affinity, fast internalization, and localization at the centrosome combined with the high cytotoxicity of DM1 can provide significant advantages for the development of the anti-PSMA 5D3-DM1-based ADC that targets PSMA(+) PC cells by mitotic arrest, leading to cell death.

2. MATERIALS AND METHODS

2.1. Antibody, Chemicals, and Reagents.

Anti-PSMA mAb, 5D3 was produced following the protocol described previously and stored in 0.02% NaN_3/phosphate-buffered saline (PBS).[24] The drug, DM1, was purchased from Abcam, Inc. The heterobifunctional linker, sulfosuccinimidyl 4-(*N*-maleimidomethyl)cyclohexane-1-carboxylate (Sulfo-SMCC), amine-reactive fluorophores, Dulbecco's phosphate-buffered saline (DPBS), and BupH phosphate-buffered-saline were purchased from Thermo Fisher, Inc., and rhodamine B isothiocyanate–dextran (70 kDa) was purchased from Sigma-Aldrich, Inc. All organic solvents were of HPLC-grade, purchased from Fisher Scientific, and used without further purification.

2.2. Synthesis of ADC.

The 5D3 mAb was buffer-exchanged from 0.02% NaN_3/PBS into 2 mM ethylenediaminetetraacetate (EDTA)/BupH PBS (pH 7.2) by 30 kDa MWCO ultracentrifugation filtration. A fraction of the 5D3 sample (5 mg in 1.0 mL of 2 mM EDTA/BupH PBS) was treated with freshly prepared Sulfo-SMCC [10-fold molar excess, 0.15 mg in 10 μL of anhydrous dimethyl sulfoxide (DMSO)] and stirred at ambient temperature for 2 h. The resulting product, 5D3-MCC (2.5 mg in 1.0 mL of 2 mM EDTA/BupH PBS), was treated with a 2-fold molar excess of DM1 (0.15 mg in 10 μL of anhydrous DMSO) over the linker. The mixture was stirred at ambient temperature for 24 h. For optical imaging, unconjugated 5D3 mAb or 5D3-MCC were labeled with fluorophores using 10 molar equivalents of amine-reactive fluorophores, AlexaFluor-488-NHS or CF-680-NHS, for 1 h at room temperature.

2.3. Ultracentrifugation and MALDI-TOF Analysis.

Amicon ultracentrifugation filter units (4 or 15 mL capacity, 30 kDa MWCO) were used to exchange buffer, concentrate samples, and remove unreacted low-molecular weight reactants and byproducts after each step of the conjugation process. The samples were further purified by passing through Sephadex G-25 resin. ADCs and conjugates were also passed through a 0.22 μm membrane syringe filter for sterilization before drug administration. Molecular weights of intermediates and final products were determined using the Voyager DE-STR matrix-assisted laser desorption ionization time-of-flight (MALDITOF) mass spectrometer (Mass Spectrometry and Proteomics Facility, JHU School of Medicine). The average number of MCC heterobifunctional groups and DM1 molecules conjugated per mAb were 6 and 2.8, respectively, and were calculated based on the change in the molecular weight. The number of fluorophores conjugated per mAb was determined following the Thermo Fisher protocol for determination of the degree of labeling for amine-reactive probes. The size of ADC was measured by dynamic light scattering (DLS) using a Nano-ZS90 Zetasizer (Malvern Instruments, UK).

2.4. Cells.

PSMA(+) PC3-PIP and PSMA(–) PC3-Flu cells were used to study the binding affinity, internalization, and therapeutic efficacy *in vitro* and to generate dual-tumor mouse models. Both cell types were grown in RPMI 1640 medium (supplemented with 10% FBS and 1%

penicillin–streptomycin) and maintained in a humidified incubator at 37 °C in a 5% CO_2 atmosphere. Cells were confirmed to be free of mycoplasma contamination.

2.5. Cell Analysis by Flow Cytometry.

5D3-DM1 ADC binding affinity was tested in PC3-PIP and PC3-Flu cells seeded in a 6-well plate (0.4 million/well) and grown for 24 h to ~60% confluency. Fluorescent 5D3-DM1-AF-488 or 5D3-AF-488 (20 μg/mL) was incubated with cells for 30 min at 4 °C. Unbound excess mAbs or ADCs were washed once using DPBS, and cells were harvested by trypsinization. Cells were resuspended in buffer and fixed by 4% paraformaldehyde (PFA). Cells were analyzed on a BD LSR II flow cytometer using 488 nm laser for AlexaFluor 488. Fluorescence histograms for DM1 conjugated and unconjugated 5D3 on PSMA(±) cells were generated by FlowJo software.

2.6. *In Vitro* Optical Imaging.

Internalization and localization of 5D3 mAb and its drug conjugates were studied in PSMA(±) cells. PSMA(+) PC3-PIP or PSMA(–) PC3-Flu cells were seeded (4-well chamber slides, 0.2 million cells per well) and grown for 1–2 days to 80–90% confluency. Medium was removed in each chamber, and cells were treated with 150 μL of 20 μg/mL of 5D3-AF-488 or 5D3-DM1-AF-488 and incubated at 37 °C for 30 min, 1, 6, 12, and 24 h under 5% CO_2 in a humidity-controlled incubator. For one chamber treated with 5D3-AF-488, cells were pulsed with 70 kDa rhodamine–dextran (100 μg/mL) along with 5D3-AF-488. Cells were washed with DPBS for 5 min and fixed by 4% PFA on ice for 10 min. Nuclei were counterstained using Hoechst 33342 (10 μg/mL in H_2O at RT for 10 min) and wet-mounted. The images were collected using a Zeiss Axiovert 200 fluorescence microscope system equipped with an LSM 510-Meta confocal module and processed using Zeiss Zen software.

2.7. Cytotoxicity of 5D3-DM1 in PSMA(±) Cells.

Cytotoxicity and cell viability were assayed by treating PC3-PIP and PC3-Flu cells in 96-well plates in RPMI 1640 culture media with 5D3-DM1 ADC over a range of concentrations. Briefly, cells were seeded in a 96-well plate (2000 cells/well) and grown for 24 h to 40–50% confluency. Wells were treated with increasing concentrations of 5D3-DM1 or pure DM1 equivalent to the DM1 concentration in 5D3-DM1 ADC (1; 10; 100; 1000; 10,000; and 100,000 ng/mL). After 48 h incubation, IC_{50} values of 5D3-DM1 ADC and corresponding free DM1 were determined using the WST-8 assay (Dojindo Molecular Technologies), following the manufacturer's protocol. Briefly, cells in each well in 100 μL of the fresh media were treated with 10 μL of WST-8 reagent and incubated at 37 °C. During incubation, WST-8 tetrazolium salt is reduced by dehydrogenase in living cells, forming a yellow formazan dye with λ_{max} at 450 nm. After 3 h, the absorbance was measured at 450 nm. The concentration of the formazan dye in the media produced by dehydrogenases is directly proportional to the density of viable cells in the well. The cell viability of treated cells was normalized to readings in untreated control cells, which were considered to have 100% viability. Data were fitted, and IC_{50} values for DM1 and 5D3-DM1 were calculated using Prism (GraphPad, San Diego CA).

2.8. Human PC Animal Models.

Healthy, four-to-six-week-old, male athymic nude mice were used for this study. For PSMA(+) and PSMA(–) dual-tumor mouse models, PC3-PIP and PC3-Flu cells were grown to 70–80% confluency in RPMI 1640 media, trypsinized, and 5×10^6 cells were reconstituted in 50 μL of RPMI 1640/Matrigel (1:1) for each inoculation and maintained at 4 °C. PSMA(±) cells were subcutaneously inoculated in the left and right flanks of the animal. When each tumor volume reached 100–150 mm^3 in size, mice were used for *in vivo* imaging and therapeutic and toxicological studies. All animal experiments were carried out in accordance with protocols approved by the Johns Hopkins University Animal Care and Use Committee and were conducted in strict compliance with all federal and institutional guidelines. At the end of imaging and therapeutic experiments, mice were euthanized according to the protocol.

2.9. Determination of *In Vivo* Therapeutic Efficacy.

Four groups of male athymic nude mice, subcutaneously inoculated with PC3-PIP and PC3-Flu human PC cells, were administered three different doses of 5D3-DM1-CF-680 (1.0, 2.5, and 5.0 mg/kg in 200 μL of saline) and 200 μL of saline for the control group. Mice were imaged using a Xenogen IVIS 200 Optical Imaging system to confirm the tumor uptake of 5D3-DM1-CF-680. The second therapeutic dose was given after two weeks. The sizes of the tumors were measured with a caliper every other day during the complete treatment. The tumor volume was calculated using the formula $(L \times W^2)\pi/6$, where L is the longest diameter (the major axis) and W is the tumor width, measured perpendicular to the major axis.

2.10. Toxicological Study.

The live toxicological assessment included daily clinical observations, body weight measurements every other day, and food consumption. After the 3-week treatment, animals were euthanized and the blood was immediately collected for complete blood count (CBC) and for the analysis of the toxicological chemistry profile. Blood urea nitrogen (BUN), alanine aminotransferase (ALT), and aspartate aminotransferase (AST) were analyzed to determine the long-term liver and kidney toxicity of the drug. After euthanization, tumors and vital organs, liver, kidney, heart, spleen, lungs, sternum, small intestine, colon, and gallbladder, were extracted, preserved in 10% neutral-buffered formalin, and embedded in paraffin. H&E staining was performed on 4 μm sections following a standard protocol. Toxicology studies were carried out in treated and untreated tumor-bearing mice and healthy mice. Metastatic tumors in vital organs were also preserved for future analyses.

2.11. Statistical Analysis.

The *in vitro* therapeutic study was executed in triplicate per plate, and duplicate independent experiments were conducted for statistics. The one-way analysis of variance (ANOVA) was used for the omnibus F-test. Changes in the cell viability were considered significant (p value < 0.05) when the F value was greater than the critical value of the F-distribution. In *in vivo* experiments, the statistical analysis (t-test) between multiple-dose treated and untreated groups was performed using JMP 12.1.0 Statistical Discovery from SAS. A p value of less

than 0.05 was considered significant (*$p < 0.05$). Survival curves in Kaplan–Meier analysis use the time when the tumor has reached a four-fold increase in the volume relative to the initial tumor volume as the surrogate endpoint.

3. RESULTS

3.1. Synthesis of 5D3-DM1 ADCs.

In the synthesis of 5D3-DM1 ADC, approximately six MCC groups were conjugated per antibody molecule (Scheme 1). Two equivalents of DM1, with respect to the number of attached MCC groups, were used for the drug conjugation. The final ADC had an average of 2.8 DM1 molecules per antibody. Because DM1 is a hydrophobic molecule, a 24 h reaction time in the rotating mixer was required for this conjugation. The resulting ADC was labeled with AlexaFluor 488 or CF-680 NIR fluorophores for *in vitro* imaging and flow cytometry or *in vivo* imaging experiments, respectively. Unconjugated 5D3 mAb was also labeled with AF-488 dyes for control imaging and flow cytometry. The average number of fluorophores per antibody was maintained as approximately two. The molecular weights of 5D3-MCC and 5D3-DM1 ADC were measured by MALDI-TOF. The number of conjugated groups and drugs was determined based on the shift of molecular weights, as shown in Figure 1A. Changes in size after modifications determined by DLS were not statistically significant (Figure 1B).

3.2. Cell Analysis by Flow Cytometry.

Figure 1C shows the histograms of PC3-PIP and PC3-Flu cells treated with 5D3-DM1-AF-488 or 5D3-AF-488. PC3-PIP cells overexpress PSMA compared to PC3-Flu cells. There were no significant changes between the histograms of cells treated with 5D3-DM1-AF-488 and 5D3-AF-488, proving that the conjugation of drug molecules does not change the PSMA-specificity and binding properties of 5D3 mAb.

3.3. *In Vitro* Cellular Imaging.

PSMA(+) PC3-PIP cells were labeled with fluorescent 5D3-AF-488 and 5D3-DM1-AF-488 conjugates, and confocal images are shown in Figure 2. Both mAb and ADC were internalized quickly and localized in the cytoplasm within 30 min and remained in the cell for more than 24 h. Unlike other cancer-cell-specific antibodies (Figure S1), both 5D3 (Figure 2A) and 5D3-DM1 ADC (Figure 2B) were localized in the vicinity of the nucleus immediately after internalization. This unique behavior was further analyzed by observing dividing cells at high resolution (Figure 2C). The enlarged view in Figure 2C shows a late anaphase stage of a mitotic cell. The 5D3-AF-488 conjugate appears to be associated with the centrosomes of dividing cells. When cells are incubated with 5D3-AF-488 and co-treated with the rhodamine-B dextran (70 kDa) endosome marker, the two-color images reveal that 5D3 localization does not overlap with late endosomes and lysosomes (Figure 2D). No significant uptake of 5D3-DM1 ADC was observed in PSMA(–) PC3-Flu cells (Figure S2).

3.4. *In Vitro* Therapeutic Study.

The 5D3-DM1 ADC and unconjugated DM1 were used for microscale determination of the drug cytotoxicity in PSMA(+) PC3-PIP and PSMA(–) PC3-Flu cells (Figure 3). For the

direct comparison of cytotoxicity, the dose was normalized for DM1 concentrations in nM. The most pronounced cytotoxicity was observed for PSMA(+) PC3-PIP cells treated with 5D3-DM1, with a corresponding IC_{50} value of 0.70 nM (Figure 3A). The same drug in PSMA(–) PC3-Flu cells had an IC_{50} of 13.98 nM. Cell treatment with matching concentrations of the free DM1 drug was less toxic for both PC3-PIP and PC3-Flu cells, with IC_{50} values of 603.8 and 735.2 nM, respectively (Figure 3B). These results suggest that the cytotoxicity of 5D3-DM1 was target-mediated by the antibody.

3.5. *In Vivo* Therapeutic Efficacy.

PSMA(+) PC3-PIP and PSMA(–) PC3-Flu dual-tumor mouse models were used in this study following the treatment schedule shown in Figure 4A. In this study, we selected three doses for the treatment plan to evaluate the therapeutic efficacy of the drug. Four groups of mice were treated with increasing doses of 5D3-DM1 (1.0, 2.5, and 5.0 mg/kg, and saline as a control). The second dose was administered on day 14. On day 21, mice were euthanized and the toxicological profiles were evaluated in all mice. A day after the administration of the second dose of 5D3-DM1-CF-680, dual-tumor mice were imaged using a Xenogen IVIS 200 Optical Imaging system (Figure 4B). Compared to the untreated mice [Figure 4B(i)], 5D3-DM1-CF-680 treated mice showed a high tumor uptake by the PSMA(+) PC3-PIP tumor [Figure 4B(ii)]. The volumes of PC3-PIP tumors in 5D3-DM1-CF-680 treated mice were smaller than that of PSMA(–) or untreated tumors. Only a slight uptake of ADC was seen in the PC3-Flu tumor in the same mouse.

The therapeutic effects of 5D3-DM1-CF-680 in PSMA(+) PC3-PIP tumors are shown in Figure 5. In this study, mice treated with the highest dose of 5.0 mg/kg showed the maximum, and statistically significant, therapeutic efficacy in PSMA(+) tumors compared to all other doses; however, 5.0 mg/kg is not the maximum tolerated dose for 5D3-DM1-CF-680. As shown in Figure 5A, the relative tumor volume was significantly lower ($*p < 0.05$) from day 15 onward with respect to the untreated group. At the end of the therapy, the 2.5 mg/kg dose treatment also provided significantly higher therapeutic efficacy compared to the 1.0 mg/kg dose and saline treatment ($\#p < 0.05$) at day 21. However, the 1.0 mg/kg dose was unable to produce significant therapeutic efficacy. The treatment response of PSMA(–) PC3-Flu tumors was observed, and the results are shown in Figure 5B. Interestingly, the growth rate of PC3-Flu tumors was slightly lower compared to the untreated mice; however, it was not statistically significant at any dose regimen.

Figure 5C shows changes in relative tumor volumes among PSMA(+) PC3-PIP and PSMA(–) PC3-Flu tumors in multiple treatment groups on day 21 (end of the treatment). The overall efficacy was higher in PSMA(+) tumors and the 5.0 mg/kg dose group exhibited significantly ($*p < 0.05$) higher therapeutic efficacy in PSMA(+) tumors compared to PSMA(–) tumors. The 2.5 mg/kg treatment was not significantly efficacious when PSMA(+) and PSMA(–) tumors were compared. Overall, the 5.0 mg/kg dose showed a statistically significant therapeutic efficacy in PSMA(+) tumor models compared to all other dose treatment groups, the untreated group, and PSMA(–) tumors.

The Kaplan–Meier surrogate survival results for untreated mice and mice treated with 5D3-DM1-CF-680 are shown in Figure 5D,E. The results demonstrated that the 5.0 mg/kg

treatment increased the survival of mice with PSMA(+) tumors (*$p < 0.05$), and approximately, 50% of tumors did not reach the four-fold relative tumor size during the treatment. All other treated and untreated PSMA(+) and PSMA(–) tumors exceeded four-fold relative tumor growth before day 19.

3.6. Systemic Toxicity of the Therapy.

At day 21, mice were euthanized and blood was collected for CBC and toxicology chemical profile analyses. The CBC showed no significant change between healthy, tumor-bearing untreated, and treated mice. BUN (Figure 6A) and ALT (Figure 6B) levels in treated and untreated mice were within the normal range; however, AST (Figure 6C) was elevated in both the untreated and treated tumor-bearing groups. Mice were weighed every other day to evaluate the *in vivo* toxicity of 5D3-DM1 (Figure 6D). A slight weight loss was observed in all treated mice; however, it was insignificant compared to untreated healthy mice. The H&E staining was performed in fixed tissue samples and did not show organ toxicity of the treatment in any of the experimental mice. Figure 7 shows high necrosis in PSMA(+) PC3-PIP tumors (Figure 7A) compared to PSMA(–) PC3-Flu tumors (Figure 7B), the animal group treated with the 5.0 mg/kg dose. However, we observed necrosis in both tumor models that is typically observed in large experimental tumors. We observed no tissue damage in the liver and kidney of mice treated with the 5.0 mg/kg dose (Figure 7C).

4. DISCUSSION

PSMA is widely used as a biomarker to image PC, drug delivery, and radioligand therapy.[32–35] PSMA-specific small molecules, peptides, and mAbs are used as the bioligands with which to target PSMA. The 5D3 antibody has a sub-nanomolar affinity for PSMA, and we have previously used this antibody for pretargeting therapy and proved the concept *in vitro*. The *in vivo* pretargeting therapy with 5D3 mAb is challenging because of its fast internalization rates. Nevertheless, high target-specificity and affinity, together with the fast internalization rate, make 5D3 mAb an ideal bioligand with which to target PSMA and serve as a platform for the development of therapeutics. In addition, after internalization, 5D3 localizes to the centrosome, an organelle critical for cell division. The centrosome organizes microtubules during cell division; hence, 5D3 is ideal for delivering anti-tubulin agents to this organelle. We are currently studying the specific mechanisms that drive 5D3 localization to centrosomes and suggest that a receptor-mediated specificity is involved in this phenomenon.

The anti-tubulin agent, DM1, has been successfully used for the development of ADC to treat other cancers. For example, trastuzumab- and DM1-based T-DM1, developed through amine conjugation chemistry, is a novel FDA-approved ADC used to treat HER2(+) breast cancer (IC_{50} = 0.22–4.26 nM).[36] PSMA-targeting small therapeutic molecules have also been tested to treat PSMA(+) PC, and most of them have an IC_{50} in the nanomolar range (1–800 nM).[37] Nevertheless, DM1 is still a popular drug in ADC development.[29] In T-DM1, the anti-HER2 trastuzumab is conjugated with DM1 through an MCC linker. We used the same MCC conjugation chemistry in 5D3-DM1 development, rather than a disulfide linkage to avoid the rapid dissociation as seen with the MLN2704.[22] There was no significant

degradation of 5D3-DM1 observed in PBS storing for 9 months at 4 °C (Figure S3). The complete stability test for 5D3-DM1 in PBS and plasma will be performed in the future.

In 5D3-DM1 ADC synthesis, 5D3 mAb was first functionalized with maleimide groups by conjugation with an MCC linker using amine-NHS ester conjugation chemistry. Amino groups are common in proteins, and this conjugation chemistry is widely used for mAb modification with drugs and imaging agents. Non-specificity and lack of control in the reaction are challenges in amine conjugation of mAbs. Amine conjugation also has limited control in maintaining the reproducibility of the drug loading. We judiciously maintained the reaction conditions, such as molar equivalent, concentration of reactants, pH, agitation, and temperature, to ensure the consistency of drug loading. The number of MCC groups per mAb was limited to six. After purification, two equivalents of DM1, with respect to the total molar content of MCC groups in the reaction, were reacted with 5D3-MCC. Precise control and maintenance of the MCC load and equivalents of the reactants are important so that the mAb is not overloaded with hydrophobic DM1 that could lead to mAb precipitation. Batches of unconjugated 5D3 and 5D3-DM1 ADCs were labeled with suitable fluorophores for direct *in vitro* and *in vivo* optical imaging. Therefore, the mAb and its conjugates could be tracked without the use of secondary antibodies.

The molecular weights of 5D3-MCC and 5D3-DM1 were measured by MALDI-TOF. The number of conjugated moieties per mAb was calculated based on the shifts in molecular weights. We performed flow cytometry analysis to observe any adverse changes in 5D3 for PSMA upon conjugation. Flow cytometry results revealed that there was no change in the PSMA labeling properties of 5D3 after modification. In this study, the total conjugation in fluorescent 5D3-DM1 was maintained at no more than 12 groups per antibody. For comparison, we and others have previously observed that up to 20 foreign groups can be substituted per trastuzumab without altering its binding affinity.[38–40]

Unlike other antibodies, which follow receptor-mediated clathrin endocytosis, 5D3 mAb almost immediately localizes to the vicinity of the nucleus (Figure 2C). The same phenomenon was observed after 5D3 was conjugated with DM1 to form 5D3-DM1 ADCs. High-resolution confocal images of mitotic cells revealed that 5D3 mAb localizes to the centrosome. We postulate that specific delivery of anti-tubulin agents to the centrosomes is a crucial factor for the success of 5D3 ADC therapy. Images of PC3-PIP cells treated with 5D3-AF-488 and rhodamine-labeled dextran to distinguish the centrosome and endosome compartments revealed that these compounds are localized in different cellular compartments and that internalized 5D3 mAbs are likely localized at the centrosomes. The specific mechanisms of this phenomenon are still unresolved and are the subject of our ongoing research.

In vitro assays showed that the PSMA(+) PC3-PIP cell line is highly sensitive to treatment with the 5D3-DM1 that demonstrated the lowest IC_{50} value of 0.70 nM compared to PCMA(–) PC3-Flu cells (IC_{50} = 13.98 nM). Interestingly, the control study, using free DM1 with a dose equal to the drug content in ADC, exhibited IC_{50} values of 603.8 and 735.2 nM for PC3-PIP and PC3-Flu cells, respectively. The preclinical IC_{50} value for MLN2704 is 1.4 nM for PSMA(+) LNCaP cells compared to 61.3 nM for PSMA(–) PC3 cells.[41] Successful

results of *in vitro* studies highlighted the potential and provided the rationale to use 5D3-DM1 ADCs *in vivo* to determine the therapeutic efficacy and toxicological effects in preclinical models of PSMA(+) human PC.

We have shown that 5D3-DM1-CF-680 is effective in *in vivo* subcutaneous dual xenograft mouse models of human PC. Two doses of 2.5 and 5.0 mg/kg 5D3-DM1 ADC resulted in a significant reduction of PSMA(+) PC3-PIP tumors compared to PSMA(–) PC3-Flu tumors. However, the 1.0 mg/kg dose was not sufficient to impair tumor growth. We also observed an insignificant reduction of PSMA(–) tumors compared to untreated mice, presumably because of nonspecific accumulation and degradation of cytotoxic ADCs in the tumor due to the enhanced permeability and retention (EPR) effect.[42,43] The highest dose used in the study, 5.0 mg/kg, was below the maximum tolerated dose. However, we suggest that the high therapeutic efficacy of 5D3-DM1 in PSMA(+) tumors is attributable to the combination of efficient delivery of ADC to the tumor by the EPR effect, specific targeting of the PSMA(+) cancer cell surface receptor, and rapid internalization and intracellular delivery of the cytotoxic cargo to the centrosome within the target cancer cell. The results of the study demonstrate a significant effect of the 5D3-DM1 targeted therapy in PC3-PIP tumors treated with the 5.0 mg/kg dose compared to the low-dose treatments ($*p < 0.05$). Fifty percent of PSMA(+) PC animals survived without reaching the surrogate survival endpoint (four times the initial tumor volume) during the 21 day treatment with 5.0 mg/kg 5D3-DM1. In all other groups treated with lower doses, including PSMA(–) models, tumors reached four times the initial tumor volume limit before the therapy was completed.

No clinical manifestations of systemic toxicity were detected in mice treated with 5D3-DM1. During the course of the treatment, the mean body weight of mice in each treatment group remained practically unchanged, including healthy mice and mice treated with 5D3-DM1 (Figure 6D). The platelet (PLT) count dropped, and the white blood cell (WBC) count was elevated after treatment; however, all counts were still within the healthy range (Figure S4).

We observed no pathological alterations in liver, kidney, heart, spleen, lungs, sternum, small intestine, colon, or gallbladder in treated animals. Metastatic tumors were observed in the kidneys of untreated mice (Figure S5) but not in treated mice. Considerably large necrotic areas were seen in both treated and untreated PSMA(+) and PSMA(–) (Figure 7). The inner regions of solid tumors received insufficient blood supply, resulting in oxygen and glucose deprivation and necrosis.[44–47] Hence, we believe that extensive necrosis in the core of untreated and PSMA(–) tumors is due to these ischemic conditions.

5. CONCLUSIONS

We have developed a novel ADC for the treatment of PC using the high target-specificity, binding affinity, and centrosomal localization of anti-PSMA 5D3 mAb and high cytotoxicity of DM1. The 5D3-DM1 ADC labeled with imaging agents demonstrated a high and homogeneous tumor uptake in PSMA(+) tumors. The 5D3-DM1 conjugates also resulted in a high tumor response without any notable adverse systemic effects. Antibody modification using amine functional groups did not alter its binding with PSMA. Two cycles of treatment

using a 5.0 mg/kg dose provided efficient control of PSMA(+) tumor growth, which resulted in 50% of mice surpassing the 21 day duration of the study. The treatment was also safe, as, in our studies, we observed no clinical manifestations, weight loss, or adverse changes in the CBC and blood chemistry of the treatment groups, except for the elevation of the AST level and the reduction of the PLT count due to complications of large tumors. The H&E of vital organs, including the liver and kidney, did not show any necrosis or tissue damage. Almost all tumors have a necrotic core induced by oxygen and glucose deprivation at the end of treatment. Based on our experimental results, we are confident that 5D3-DM1 can become a new and highly efficacious therapy for aggressive PC. We envision future clinical applications of this strategy, which will increase the therapeutic efficacy while minimizing the systemic toxicity in PC patients possibly before metastasis into vital organs and bones.

Supplementary Material

Refer to Web version on PubMed Central for supplementary material.

ACKNOWLEDGMENTS

This study was mainly supported by the Emerson Collective Cancer Research Fund (2018 Emerson Collective 128821). This work was partially supported by the DOD (W81XWH-16-1-0595), the NIH/NCI R01CA209884, and the NIH/NIBIB (P41EB024495). This work was, in part, supported by the CAS (RVO: 86652036), CSF (18-04790S), and IOCEV/ERDF (CZ.1.05/1.1.00/02.0109). The authors acknowledge Dixie Hoyle and Zora Novakova for their assistance in flow cytometry and antibody purification, respectively.

ABBREVIATIONS

ADC	antibody-drug conjugate
DM1	mertansine
DPBS	Dulbecco’s phosphate buffered saline
mAb	monoclonal antibody
MALDI-TOF	matrix-assisted laser desorption ionization time-of-flight mass spectrometry
PBS	BupH phosphate buffered saline
PC	prostate cancer
PSMA	prostate-specific membrane antigen
SEC	size-exclusion chromatography
Sulfo-SMCC	sulfosuccinimidyl 4-(*N*-maleimidomethyl)cyclohexane-1-carboxylate

REFERENCES

(1). Siegel RL; Miller KD; Jemal A Cancer Statistics, 2019. Ca—Cancer J. Clin 2019, 69, 7–34. [PubMed: 30620402]

(2). Siegel RL; Miller KD; Jemal A Cancer Statistics, 2020. Ca—Cancer J. Clin 2020, 70, 7–30. [PubMed: 31912902]

(3). Cho S; Zammarchi F; Williams DG; Havenith CEG; Monks NR; Tyrer P; D'Hooge F; Fleming R; Vashisht K; Dimasi N; et al. Antitumor Activity of Medi3726 (Adct-401), a Pyrrolobenzodiazepine Antibody-Drug Conjugate Targeting Psma, in Preclinical Models of Prostate Cancer. Mol. Cancer Ther 2018, 17, 2176–2186. [PubMed: 30065100]

(4). Semenas J; Allegrucci C; Boorjian S; Mongan N; Liao Persson J Overcoming Drug Resistance and Treating Advanced Prostate Cancer. Curr. Drug Targets 2012, 13, 1308–1323. [PubMed: 22746994]

(5). Phillips RM; Deek MP; Deweese TL; Tran PT Metastasis-Directed Therapy in Prostate Cancer. Why, When, and How? Oncology, 2019, 33, 394–399.

(6). Antonarakis ES; Lu C; Wang H; Luber B; Nakazawa M; Roeser JC; Chen Y; Mohammad TA; Chen Y; Fedor HL; et al. Ar-V7 and Resistance to Enzalutamide and Abiraterone in Prostate Cancer. N. Engl. J. Med 2014, 371, 1028–1038. [PubMed: 25184630]

(7). Dong L; Zieren RC; Xue W; de Reijke TM; Pienta KJ Metastatic Prostate Cancer Remains Incurable, Why? Asian J. Urol. 2019, 6, 26–41. [PubMed: 30775246]

(8). Mangadlao JD; Wang X; McCleese C; Escamilla M; Ramamurthy G; Wang Z; Govande M; Basilion JP; Burda C Prostate-Specific Membrane Antigen Targeted Gold Nanoparticles for Theranostics of Prostate Cancer. ACS Nano 2018, 12, 3714–3725. [PubMed: 29641905]

(9). Niaz MO; Sun M; Ramirez-Fort MK; Niaz MJ Prostate-Specific Membrane Antigen Based Antibody-Drug Conjugates for Metastatic Castration-Resistance Prostate Cancer. Cureus 2020, 12, No. e7147. [PubMed: 32257692]

(10). Israeli RS; Powell CT; Corr JG; Fair WR; Heston WD Expression of the Prostate-Specific Membrane Antigen. Cancer Res 1994, 54, 1807–1811. [PubMed: 7511053]

(11). Lv Q; Yang J; Zhang R; Yang Z; Yang Z; Wang Y; Xu Y; He Z Prostate-Specific Membrane Antigen Targeted Therapy of Prostate Cancer Using a Dupa-Paclitaxel Conjugate. Mol. Pharm 2018, 15, 1842–1852. [PubMed: 29608845]

(12). Wright GL Jr.; Mayer Grob B; Haley C; Grossman K; Newhall K; Petrylak D; Troyer J; Konchuba A; Schellhammer PF; Moriarty R Upregulation of Prostate-Specific Membrane Antigen after Androgen-Deprivation Therapy. Urology 1996, 48, 326–334. [PubMed: 8753752]

(13). Chang SS Overview of Prostate-Specific Membrane Antigen. Rev. Urol 2004, 6, S13–S18.

(14). Rajasekaran SA; Anilkumar G; Oshima E; Bowie JU; Liu H; Heston W; Bander NH; Rajasekaran AK A Novel Cytoplasmic Tail Mxxxl Motif Mediates the Internalization of Prostate-Specific Membrane Antigen. Mol. Biol. Cell 2003, 14, 4835–4845. [PubMed: 14528023]

(15). Dorff TB; Fanti S; Farolfi A; Reiter RE; Sadun TY; Sartor O The Evolving Role of Prostate-Specific Membrane Antigen-Based Diagnostics and Therapeutics in Prostate Cancer. Am. Soc. Clin. Oncol. Educ. Book 2019, 39, 321–330. [PubMed: 31099673]

(16). Giesel FL; Sterzing F; Schlemmer HP; Holland-Letz T; Mier W; Rius M; Afshar-Oromieh A; Kopka K; Debus J; Haberkorn U; et al. Intra-Individual Comparison of (68)Ga-Psma-11-Pet/Ct and Multi-Parametric Mr for Imaging of Primary Prostate Cancer. Eur. J. Nucl. Med. Mol. Imag 2016, 43, 1400–1406.

(17). Schwarzenboeck SM; Rauscher I; Bluemel C; Fendler WP; Rowe SP; Pomper MG; Asfhar-Oromieh A; Herrmann K; Eiber M Psma Ligands for Pet Imaging of Prostate Cancer. J. Nucl. Med 2017, 58, 1545–1552. [PubMed: 28687599]

(18). Kelly J; Amor-Coarasa A; Nikolopoulou A; Kim D; Williams C Jr.; Ponnala S; Babich JW Synthesis and Pre-Clinical Evaluation of a New Class of High-Affinity (18)F-Labeled Psma Ligands for Detection of Prostate Cancer by Pet Imaging. Eur. J. Nucl. Med. Mol. Imag 2017, 44, 647–661.

(19). Pan M-H; Gao D-W; Feng J; He J; Seo Y; Tedesco J; Wolodzko JG; Hasegawa BH; Franc BL Biodistributions of 177lu- and 111in-Labeled 7e11 Antibodies to Prostate-Specific Membrane Antigen in Xenograft Model of Prostate Cancer and Potential Use of 111in-7e11 as a Pre-Therapeutic Agent for 177lu-7e11 Radioimmunotherapy. Mol. Imag. Biol 2009, 11, 159–166.

(20). Troyer JK; Beckett ML; Wright GL Jr. Location of Prostate-Specific Membrane Antigen in the Lncap Prostate Carcinoma Cell Line. Prostate 1997, 30, 232–242. [PubMed: 9111600]

(21). Horoszewicz JS; Kawinski E; Murphy GP Monoclonal Antibodies to a New Antigenic Marker in Epithelial Prostatic Cells and Serum of Prostatic Cancer Patients. Anticancer Res 1987, 7, 927–935. [PubMed: 2449118]

(22). Milowsky MI; Galsky MD; Morris MJ; Crona DJ; George DJ; Dreicer R; Tse K; Petruck J; Webb IJ; Bander NH; et al. Phase 1/2 Multiple Ascending Dose Trial of the Prostate-Specific Membrane Antigen-Targeted Antibody Drug Conjugate Mln2704 in Metastatic Castration-Resistant Prostate Cancer. Urol. Oncol 2016, 34, 530.e515–530.e521.

(23). Banerjee SR; Kumar V; Lisok A; Plyku D; Nováková Z; Brummet M; Wharram B; Barinka C; Hobbs R; Pomper MG Evaluation of (111)in-Dota-5d3, a Surrogate Spect Imaging Agent for Radioimmunotherapy of Prostate-Specific Membrane Antigen. J. Nucl. Med 2019, 60, 400–406. [PubMed: 30237212]

(24). Nováková Z; Foss CA; Copeland BT; Morath V; Baranová P; Havlínová B; Skerra A; Pomper MG; Barinka C Novel Monoclonal Antibodies Recognizing Human Prostate-Specific Membrane Antigen (Psma) as Research and Theranostic Tools. Prostate 2017, 77, 749–764. [PubMed: 28247415]

(25). Hapuarachchige S; Huang CT; Donnelly MC; Bařinka C; Lupold SE; Pomper MG; Artemov D Cellular Delivery of Bioorthogonal Pretargeting Therapeutics in Psma-Positive Prostate Cancer. Mol. Pharm 2020, 17, 98–108. [PubMed: 31840521]

(26). Kupchan SM; Komoda Y; Court WA; Thomas GJ; Smith RM; Karim A; Gilmore CJ; Haltiwanger RC; Bryan RF Tumor inhibitors. LXXIII. Maytansine, a Novel Antileukemic Ansa Macrolide from Maytenus Ovatus. J. Am. Chem. Soc 1972, 94, 1354–1356. [PubMed: 5062169]

(27). Peddi PF; Hurvitz SA Trastuzumab Emtansine: The First Targeted Chemotherapy for Treatment of Breast Cancer. Future Oncol 2013, 9, 319–326. [PubMed: 23469968]

(28). Kupchan SM; Komoda Y; Branfman AR; Sneden AT; Court WA; Thomas GJ; Hintz HPJ; Smith RM; Karim A; Howie GA; et al. Tumor inhibitors. 122. The Maytansinoids. Isolation, Structural Elucidation, and Chemical Interrelation of Novel Ansa Macrolides. J. Org. Chem 1977, 42, 2349–2357. [PubMed: 874612]

(29). Lopus M Antibody-Dm1 Conjugates as Cancer Therapeutics. Canc. Lett 2011, 307, 113–118.

(30). Lopus M; Oroudjev E; Wilson L; Wilhelm S; Widdison W; Chari R; Jordan MA Maytansine and Cellular Metabolites of Antibody-Maytansinoid Conjugates Strongly Suppress Microtubule Dynamics by Binding to Microtubules. Mol. Cancer Ther 2010, 9, 2689–2699. [PubMed: 20937594]

(31). Rong L; Zhou S; Liu X; Li A; Jing T; Liu X; Zhang Y; Cai S; Tang X Trastuzumab-Modified Dm1-Loaded Nanoparticles for Her2(+) Breast Cancer Treatment: An in Vitro and in Vivo Study. Artif. Cells, Nanomed., Biotechnol 2018, 46, 1708–1718. [PubMed: 29069935]

(32). Zimmerman ME; Meyer AR; Rowe SP; Gorin MA Imaging of Prostate Cancer with Positron Emission Tomography. Clin. Adv. Hematol. Oncol 2019, 17, 455–463. [PubMed: 31449514]

(33). Rowe SP; Drzezga A; Neumaier B; Dietlein M; Gorin MA; Zalutsky MR; Pomper MG Prostate-Specific Membrane Antigen-Targeted Radiohalogenated Pet and Therapeutic Agents for Prostate Cancer. J. Nucl. Med 2016, 57, 90S–96S. [PubMed: 27694179]

(34). Current K; Meyer C; Magyar CE; Mona CE; Almajano J; Slavik R; Stuparu AD; Cheng C; Dawson DW; Radu CG; et al. Investigating Psma-Targeted Radioligand Therapy Efficacy as a Function of Cellular Psma Levels and Intratumoral Psma Heterogeneity. Clin. Cancer Res 2020, 26, 2946–2955. [PubMed: 31932492]

(35). Müller C; Umbricht CA; Gracheva N; Tschan VJ; Pellegrini G; Bernhardt P; Zeevaart JR; Koster U; Schibli R; van der Meulen NP Terbium-161 for Psma-Targeted Radionuclide Therapy of Prostate Cancer. Eur. J. Nucl. Med. Mol. Imag 2019, 46, 1919–1930.

(36). Phillips GDL; Li G; Dugger DL; Crocker LM; Parsons KL; Mai E; Blattler WA; Lambert JM; Chari RV; Lutz RJ; et al. Targeting Her2-Positive Breast Cancer with Trastuzumab-Dm1, an Antibody-Cytotoxic Drug Conjugate. Cancer Res 2008, 68, 9280–9290. [PubMed: 19010901]

(37). Machulkin AE; Ivanenkov YA; Aladinskaya AV; Veselov MS; Aladinskiy VA; Beloglazkina EK; Koteliansky VE; Shakhbazyan AG; Sandulenko YB; Majouga AG Small-Molecule Psma Ligands. Current State, Sar and Perspectives. J. Drug Target 2016, 24, 679–693. [PubMed: 26887438]

(38). Hapuarachchige S; Kato Y; Artemov D Bioorthogonal Two-Component Drug Delivery in Her2(+) Breast Cancer Mouse Models. Sci. Rep 2016, 6, 24298. [PubMed: 27068794]

(39). Hapuarachchige S; Zhu W; Kato Y; Artemov D Bioorthogonal, Two-Component Delivery Systems Based on Antibody and Drug-Loaded Nanocarriers for Enhanced Internalization of Nanotherapeutics. Biomaterials 2014, 35, 2346–2354. [PubMed: 24342725]

(40). Haun JB; Devaraj NK; Hilderbrand SA; Lee H; Weissleder R Bioorthogonal Chemistry Amplifies Nanoparticle Binding and Enhances the Sensitivity of Cell Detection. Nat. Nanotechnol 2010, 5, 660–665. [PubMed: 20676091]

(41). Galsky MD; Eisenberger M; Moore-Cooper S; Kelly WK; Slovin SF; DeLaCruz A; Lee Y; Webb IJ; Scher HI Phase I Trial of the Prostate-Specific Membrane Antigen-Directed Immunoconjugate Mln2704 in Patients with Progressive Metastatic Castration-Resistant Prostate Cancer. J. Clin. Oncol 2008, 26, 2147–2154. [PubMed: 18362364]

(42). Kobayashi H; Choyke PL Super Enhanced Permeability and Retention (Supr) Effects in Tumors Following near Infrared Photoimmunotherapy. Nanoscale 2016, 8, 12504–12509. [PubMed: 26443992]

(43). Nakamura Y; Mochida A; Choyke PL; Kobayashi H Nanodrug Delivery: Is the Enhanced Permeability and Retention Effect Sufficient for Curing Cancer? Bioconjugate Chem. 2016, 27, 2225–2238.

(44). Lee SY; Ju MK; Jeon HM; Jeong EK; Lee YJ; Kim CH; Park HG; Han SI; Kang HS Regulation of Tumor Progression by Programmed Necrosis. Oxid. Med. Cell. Longevity 2018, 2018, 3537471.

(45). Tomes L; Emberley E; Niu Y; Troup S; Pastorek J; Strange K; Harris A; Watson PH Necrosis and Hypoxia in Invasive Breast Carcinoma. Breast Canc. Res. Treat 2003, 81, 61–69.

(46). Cheville JC; Lohse CM; Zincke H; Weaver AL; Blute ML Comparisons of Outcome and Prognostic Features among Histologic Subtypes of Renal Cell Carcinoma. Am. J. Surg. Pathol 2003, 27, 612–624. [PubMed: 12717246]

(47). Jin S; DiPaola RS; Mathew R; White E Metabolic Catastrophe as a Means to Cancer Cell Death. J. Cell Sci 2007, 120, 379–383. [PubMed: 17251378]

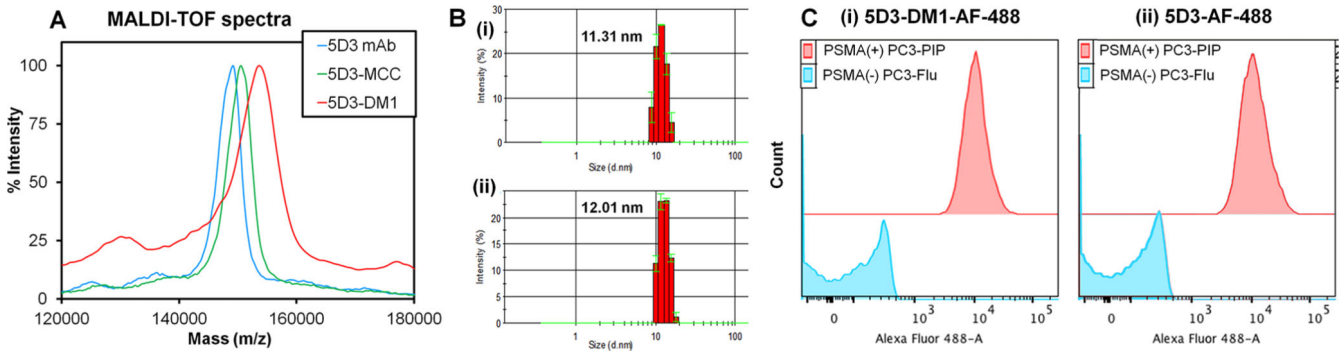

Figure 1.

Characterization of 5D3-DM1 ADC. (A) MALDI-TOF spectra of 5D3 mAb, intermediate 5D3-MCC, and 5D3-DM1 ADC. (B) DLS analysis and size distribution of 5D3 mAb (i) and 5D3-DM1 (ii). (C) Fused flow cytometric histogram of PSMA(+) PC3-PIP and PSMA(–) PC3-Flu cells labeled with 5D3-DM1-AF-488 (i) and 5D3-AF-488 (ii), showing that there is no change in the PSMA labeling properties of 5D3 after modification. Note: Histograms were plotted in red (PC3-PIP cells) and blue (PC3-Flu cells) for both 5D3-DM1-AF-488 and 5D3-AF-488 for direct comparison.

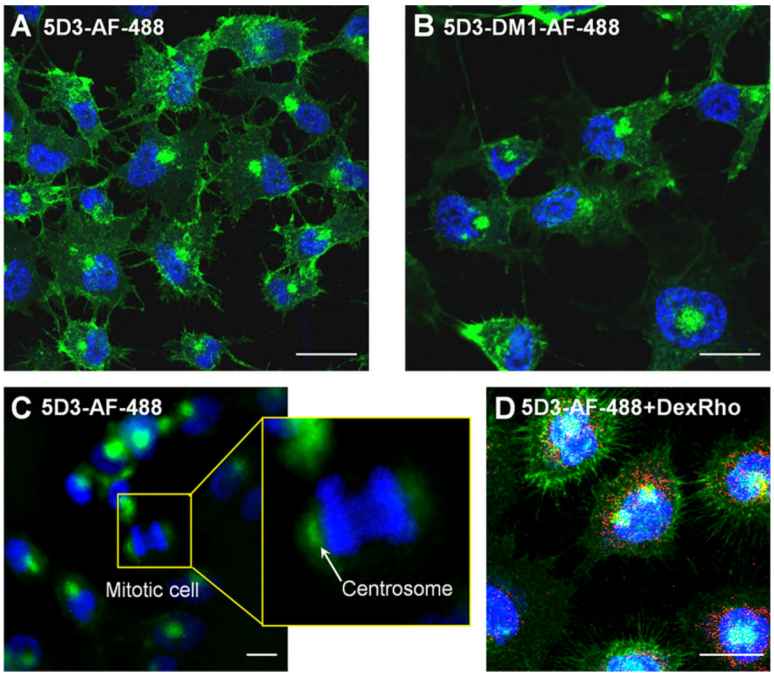

Figure 2.

Confocal fluorescence images of 5D3 mAb and 5D3-DM1 ADC in PSMA(+) PC3-PIP cells. Internalized 5D3-AF-488 (A) and 5D3-DM1-AF-488 (B) after 1 h. (C) Perinuclear localization of 5D3-AF-488. (D) Cells treated with 5D3-AF-488 (green) and dextran–rhodamine (red, visualizing endosomes), a dividing cell exhibiting the mAbs localized to the centrosomes. (Scale bar: 50 μm).

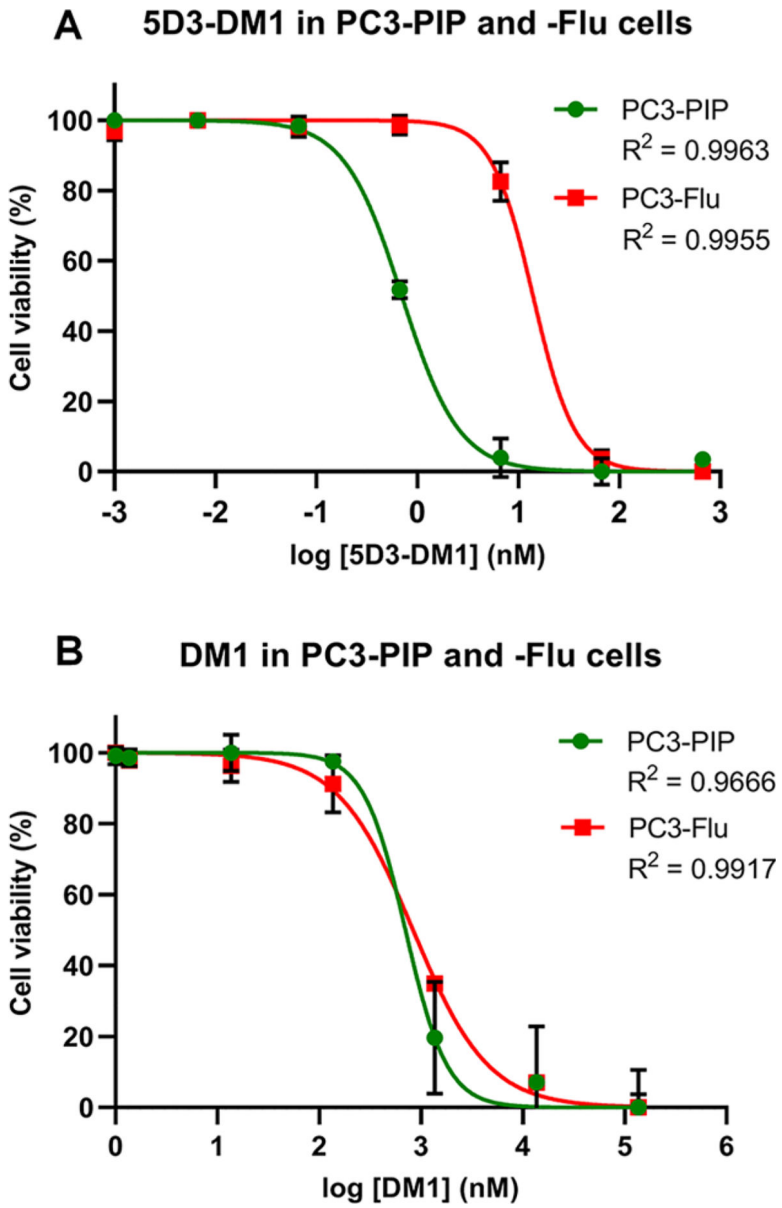

Figure 3.

In vitro cytotoxicity in PC3-PIP and PC3-Flu cells. (A) Cytotoxicity of 5D3-DM1 in PSMA(+) PC3-PIP (IC_{50} = 0.70 nM) and PSMA(–) PC3-Flu (IC_{50} = 13.98 nM) cells. (B) Cytotoxicity of DM1 equivalent to 5D3-DM1 in PSMA(+) PC3-PIP (IC_{50} = 603.8 nM) and PSMA(–) PC3-Flu (IC_{50} = 735.2 nM) cells. IC_{50} values were calculated using the GraphPad/Prism software.

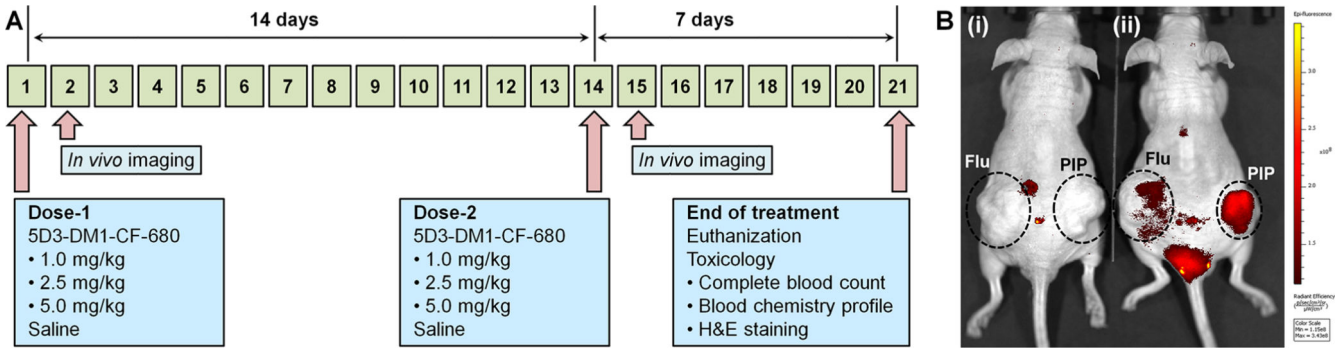

Figure 4.

In vivo therapeutic study. (A) Dosing schedule of *in vivo* therapy, imaging, and toxicological study. (B) *In vivo* NIR fluorescence images of drug delivery. The tumor uptake of 5D3-DM1-CF-680 in PSMA(+) PC3-PIP and PSMA(–) PC3-Flu dual-tumor mouse models. (i) Untreated and (ii) treated with 2.5 mg/kg of 5D3-DM1-CF-680. Images were obtained 24 h after the administration of ADC at day 15.

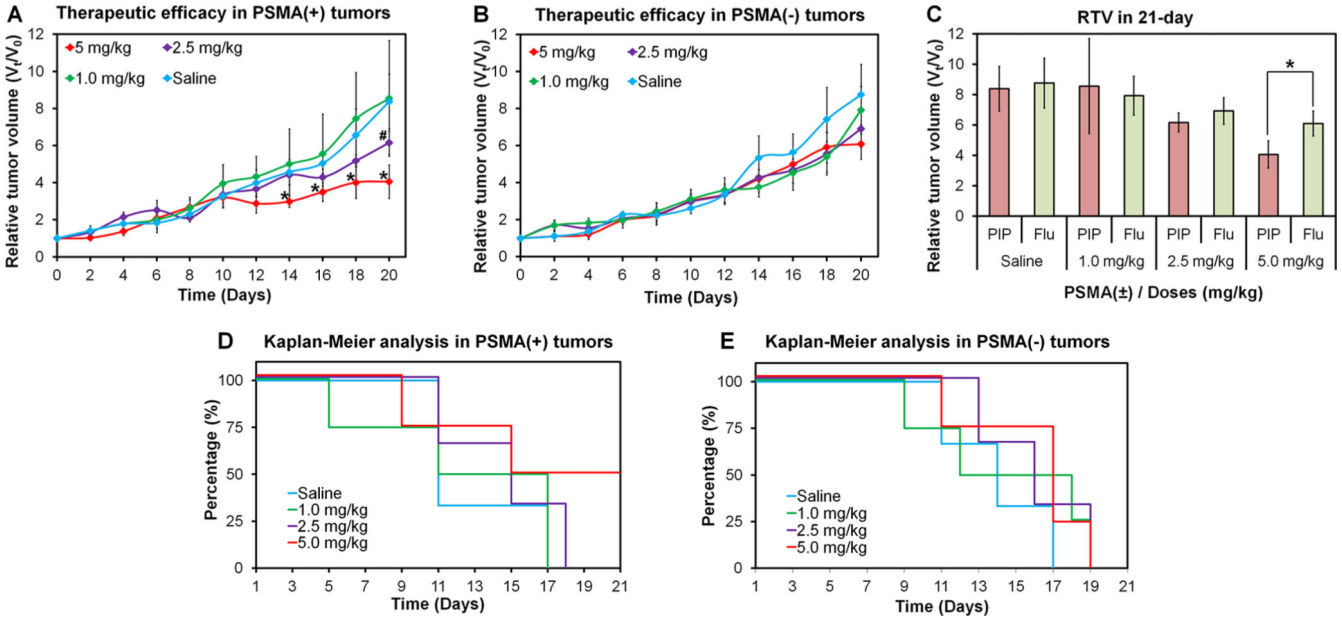

Figure 5.

In vivo therapeutic effect of 5D3-DM1-CF-680 in human PC xenograft mouse models (n = 6/group). Therapeutic efficacy of 5D3-DM1-CF-680 (1.0, 2.5, and 5.0 mg/kg) in (A) PSMA(+) PC3-PIP PC tumors and (B) PSMA(–) PC3-Flu PC tumors in mouse models. (C) Relative tumor volumes at day 21 in mice treated with multiple-doses for PC3-PIP and PC3-Flu tumors. The Kaplan–Meier analysis of the surrogate survival. Kaplan–Meier graphs were plotted using the time taken to reach four times the initial tumor size as the endpoint in (D) PSMA(+) PC3-PIP PC tumors and (E) PSMA(–) PC3-Flu PC tumors in mouse models (n = 10/group).

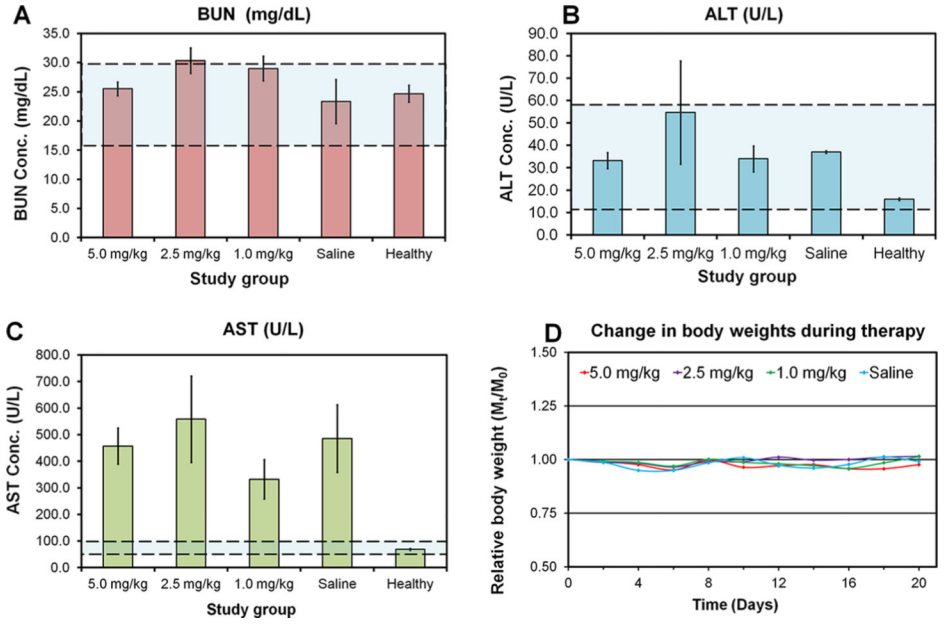

Figure 6.

Toxicological study of 5D3-DM1-CF-680 ADC therapy (n = 4/group). (A) BUN (healthy range 16–30 mg/dL), (B) ALT (healthy range 15–60 U/L), (C) AST (healthy range 50–100 U/L) concentrations for ADC-treated and saline-treated in PSMA(+) PC3-PIP and PSMA(–) PC3-Flu dual-tumor mouse models, and (D) changes in the animal body weight during the therapy relative to the initial body weight (n = 6/group).

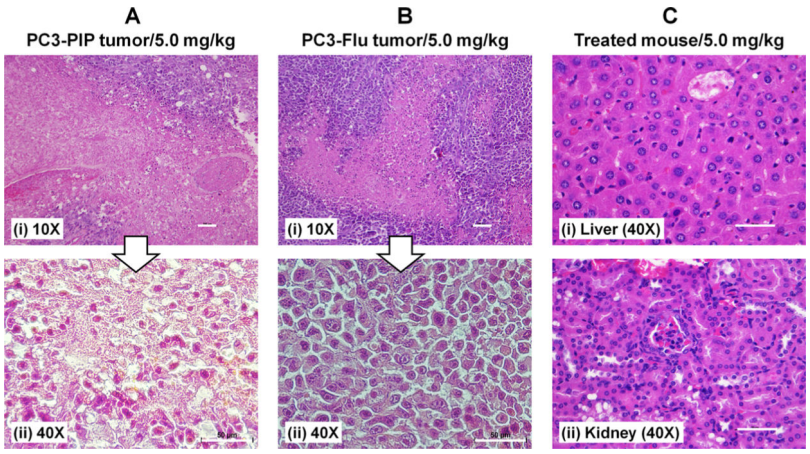

Figure 7.

H&E staining of tumors and organs in a 5.0 mg/kg dose-treated mouse. (A) PSMA(+) tumor at 10× (i) and 40× (ii). (B) PSMA(–) tumor at 10× (i) and 40× (ii). (C) Liver tissue (i) and kidney tissue (ii) at 40×. Study shows high necrosis in the PSMA(+) PC3-PIP tumor, low necrosis in the PSMA(–) PC3-Flu tumor, and no toxicological damage in the liver or kidney. (Scale bars: 100 μm in 10× images and 50 μm in 40× images).

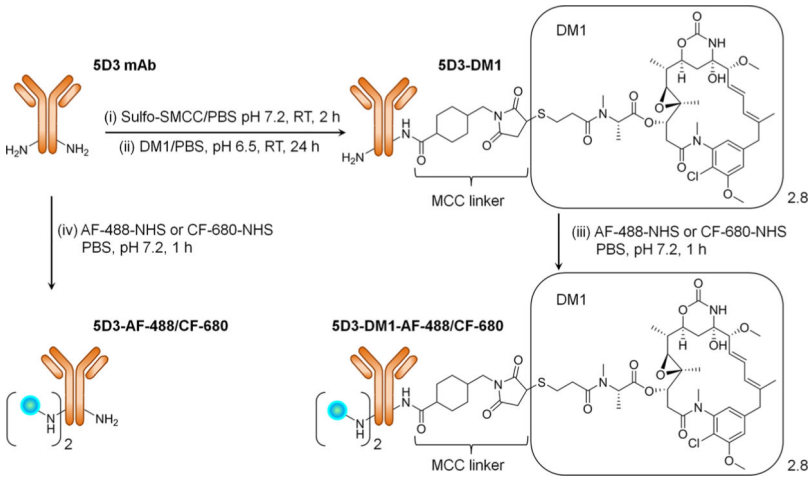

Scheme 1. Synthesis of the 5D3-DM1 ADC and Its Fluorescence Analogues[a]

[a]In the first step, 5D3 mAb was functionalized by reaction with the Sulfo-SMCC heterobifunctional linker (i) and conjugated with DM1 (ii). The resulting 5D3-DM1 (iii) and 5D3 mAbs (iv) were labeled with AF-488 (for *in vitro* imaging and flow cytometric analysis) or CF-680 (for *in vivo* optical imaging).